Ultraviolet-laser-induced periodic surface structures

S. E. Clark and D. C. Emmony
Department of Physics, Loughborough University of Technology, Loughborough, Leicestershire LE11 3TU, United Kingdom
(Received 10 August 1988; revised manuscript received 13 February 1989)

We report the first systematic investigation into the properties of ultraviolet-laser-induced periodic surface structures that can be produced on nominally smooth surfaces. The study investigates the dependence of the patterns that are produced on Ge and Al by a KrF 249-nm laser on incident fluence and both the polarization and angle of incidence of the light. At high fluence we show that the results are consistent with the assumption that the surface melts uniformly, whereas the patterns formed at low fluence can be explained on the basis of the localized melting of the surface. For *P*-polarized light we find two dominant patterns, one perpendicular to the polarization and one parallel to it. For *S*-polarized light we report the first observation of two new patterns, one parallel and one perpendicular to the polarization, of which the latter is explained by invoking a new formation mechanism. The results show that for *P*-polarized light at large angles of incidence the ripple spacing shows large deviations from its previously expected value. The results are shown to be in excellent agreement with a previously developed first-principles theory. In addition, we report surface structures that are consistent with the idea of capillary waves being launched and subsequently frozen on the surface of the material.

I. INTRODUCTION

Many workers have observed the phenomenon of laser-induced periodic surface structures (LIPSS), i.e., gratinglike patterns induced on the surface of materials due to the incident laser radiation (see Fig. 1, for example). The effect first reported by Birnbaum[1] has usually been observed using high-power pulsed lasers, although in notable cases,[2–3] a low-power cw beam was used. Most of the work has been performed on semiconduc-

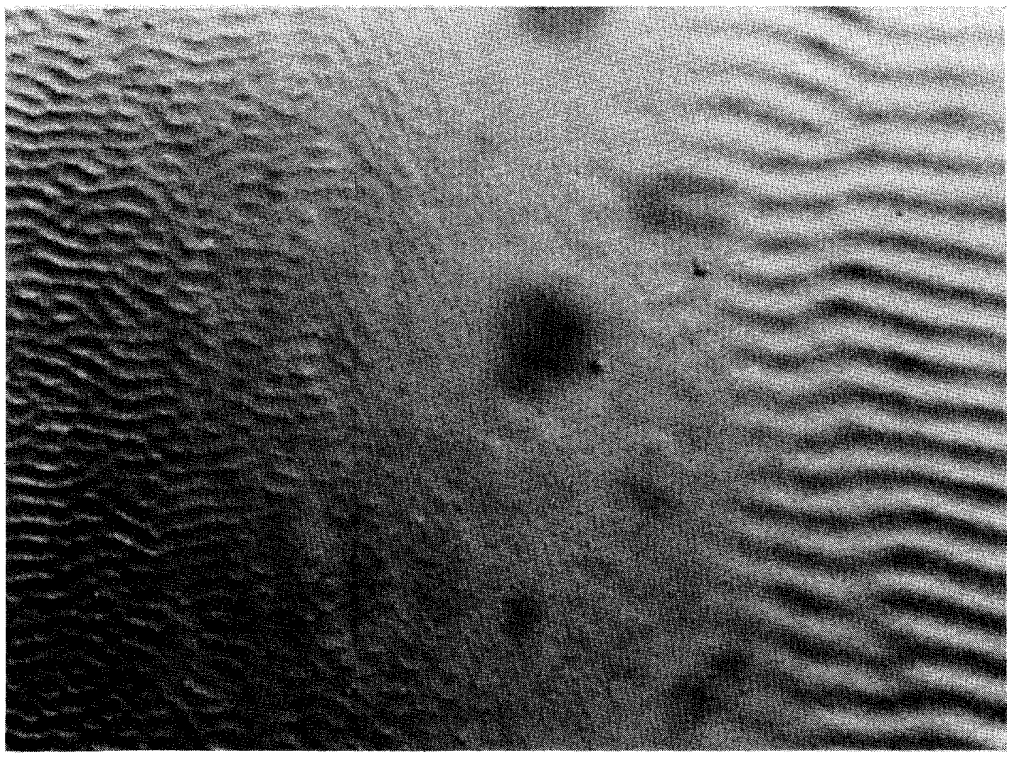

FIG. 1. Germanium sample, *P*-polarized light incident at 75°, magnification XM 2000. This micrograph shows both types of *p* fringes together with the extremely uniform *c* type orientated perpendicularly to the others. The ripples formed on the uniformly melted surface (right-hand side) appear to have a much flatter more sinusoidal shaped profile.

tors[4–8] and crystal insulators such as NaCl (Refs. 9–11) with a little on metals.[6–8,12,13]. The basis of the currently accepted theory of LIPSS, i.e., the interference of the incident light and some form of "surface scattered wave," was suggested by Emmony *et al.*[5] Subsequent modeling, notably by Temple and Solieau,[9,10] Prokhorov *et al.*,[12] Emel'yanov *et al.*,[13] and by Gousheng *et al.*[6] led to some improvement in the theoretical description of LIPSS. Substantial progress in the understanding of LIPSS resulted from the theoretical work of Sipe *et al.*,[4] (hereafter known as I), and the experimental works of Young *et al.*[7,8] (hereafter known as II and III, respectively). Although some previous work[3,14] on LIPSS at uv wavelengths has been reported, to our knowledge this is the first quantitative study to be performed at uv wavelengths, which is a region of significance, since there Ge behaves optically like a metal, whereas in most previous studies performed in the infrared it behaves as a dielectric.

The rest of the paper is organized as follows: Sec. II describes the experimental arrangement used; Sec. III lists the result obtained, whilst Sec. IV discusses the theory used in the work; Sec. V is a comparison between theory and experiment, and Sec. VI is the conclusions.

II. EXPERIMENTS

This study was performed using a Lambda Physik KrF Excimer laser operating at 249 nm producing a pulse of unpolarized light of approximately 30 ns duration. To reach the required fluences a 20 cm focal length quartz lens was used to focus the beam to an area approximately 2 by 0.5 mm^2. Control of the energy was achieved by means of a liquid dye cell attenuator so that typically 1–15 mJ of energy was incident on the target. The beam profile and fluence levels were measured using a computer-controlled video frame store system[15] that images the fluorescence produced by the excimer beam on a thin piece of absorbing glass.

Polarized light was obtained by using the reflected light from a single quartz beam splitter orientated at Brewster's angle (56°). Variation in the angle of incidence of the excimer beam for *S*-polarized light was achieved by rotating the sample with no tilt, but for *P*-polarized light by tilting the sample with no rotation. Beam profile measurements were made over a range of 5 mm either side of the working position, revealing an approximately constant spot size, thus ensuring that the profile seen by a tilted and/or rotated sample was essentially the same as that at normal incidence. In this study two materials were used, pure laser quality, polished polycrystalline germanium, and commercially pure (99%) aluminium polished initially with 3-μm diamond paste, and finally with OP-S polishing suspension.[16]

Real time detection of any changes on the surface was performed by direct visual observation of the surface. It was found that unless some form of surface breakdown (i.e., readily observable plasma) occurred, no ripples were observed even after several hundred shots. Most of the post-irradiation analysis of the modified surfaces was performed on a Reichert MeF3 optical microscope using an interference contrast technique. Attempts to view the ripples with a scanning electron microscope (SEM) proved unsuccessful, often with the SEM being unable to detect any patterns even if the sample, when viewed by eye, showed effects similar to a diffraction grating. Transmission electron microscope (TEM) studies of the rippled surfaces using a JEOL, JEM, 100 *CV*1, were performed to determine if any subwavelength structures were present to allow a comparison with the high-frequency predictions of the theory in I. To facilitate this, replicas of the surface using a standard carbon coating based replication technique were made.

III. RESULTS

Depending upon the incident excimer fluence, three types of patterns were observed. At low fluences, patterns consistent with the theory in I, i.e., LIPSS were observed. At somewhat higher fluences, it was possible to form both LIPSS and structures with a morphology consistent with the freezing in of capillary waves but with a spacing that showed no angular or polarization dependence. We shall term such structures induced capillary waves (ICW). At the highest fluences used, patterns having a similar dependence to LIPSS of their spacing and orientation on the incident excimer beam but with a much larger spacing were seen and have consequently been labeled as anomalous laser-induced periodic surface structures (ALIPSS).

A. LIPSS

LIPSS formation was found to be a function of on-target fluence, number of shots, polarization, and angle of incidence of the incident light. At low fluences or number of shots, the ripples formed in the center of the damage site, i.e., where the beam, is most intense. At higher fluences, LIPSS in the center of the damage site with spacings different to those formed in the outer edges (Fig. 1) were observed. At still higher fluences the center part became badly damaged and the ripples formed in an annulus towards the edge of the damage site. If too many shots were used, the pattern was "washed out," leaving a badly damaged site with a variety of intricate anomalous structures on it. In general, the fringes formed on Al were less well defined than their counterparts on Ge and required typically two or three times more energy to form than those on Ge, a difference that can partly be accounted for by the difference in reflectivity of Al and Ge.

Even if several hundred shots were used, no LIPSS were formed unless there was some form of laser-induced plasma. As the number of shots during which a plasma occurred increased the pattern built up and became observable after about four plasma shots, and was most distinct after some 20 to 40 shots, and then was gradually "washed" out as the number of shots increased. Even at energies which gave breakdown after 20 shots, unless there were at least four subsequent shots during which a small plasma (breakdown) occurred, there were no detectable LIPSS, although the surface was modified, typically

breaking up into small globules. If surface breakdown occurred after less than ten shots, and even if only a few subsequent shots were used, the surface was left badly damaged with no normally spaced LIPSS discernable.

In order to be consistent with the theory in I we shall specify the orientation of the induced fringes by reference to the component of incident wave vector (**kp**) that is parallel to the surface and to the so-called grating vector which is defined to be perpendicular to the fringes. Four types of patterns were observed, two each for *P*- and *S*-polarized light with each polarization having one pattern with a grating vector parallel to **kp** and one perpendicular. For *S*-polarized light (Fig. 2) the pattern with a grating vector parallel to **kp** had a spacing given by $\lambda(1-\sin\theta)^{-1}$ even for large angles. Following the nomenclature introduced in II we label these as s^--type fringes. The second pattern which is of much larger spacing was found to have a grating vector perpendicular to **kp** and have no simple dependence of its spacing on the angle of incidence of the excimer laser and for reasons to be discussed, these fringes are labeled as *b*-type fringes.

For *P*-polarized light the more common pattern has a grating vector parallel to **kp** but has a spacing that shows substantial deviations from $\lambda/(1-\sin\theta)$ at large angles, i.e., $>60°$. These fringes will be labeled as p^--type fringes. At large angles of incidence an extremely uniform set of fringes with a grating vector perpendicular to **kp** are produced with a spacing of the order of $\lambda/\cos\theta$, and again following II are labeled as *c*-type fringes. It is interesting to note that the *c*-type fringes formed at lower energies than the p^- type. Within the *p*-type fringes two distinct types of pattern with different spacings were observed at large angles (Fig. 1). The one with larger wavelength occurred in the center of the damage site where the fluence is highest, and the other towards the edge.

TEM studies revealed a variety of subwavelength structures ranging from approximately 300 to 90 nm depending upon angle of incidence, polarization, and the type of sample. Unfortunately due to both the replication process and the intrinsic rotation of the image in the TEM itself, we were unable to accurately determine the orientation of the observed fringes, only their spacing could be found. The results for LIPSS are summarized in Table I.

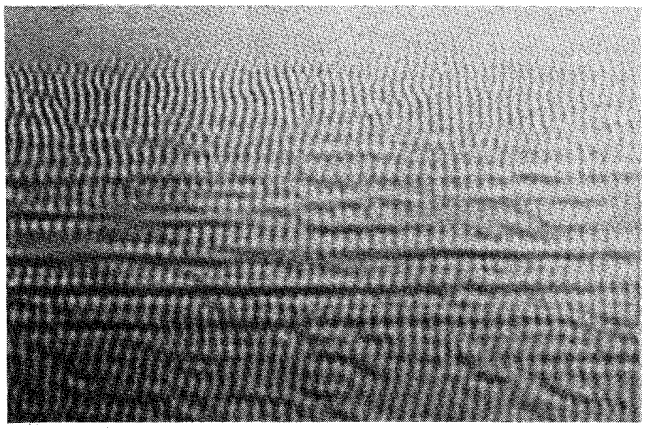

FIG. 2. Germanium sample, *S*-polarized light incident at 70°, magnification XM 1250. The variation of spacing vertically along the picture is believed to be associated with a varying dielectric constant due to a temperature gradient. Also note large near horizontal *b*-type fringes of spacing $\approx 8\,\mu$m.

B. ICW

At fluences higher than the minimum required to form LIPSS but not necessarily high enough to wash out the

TABLE I. Summary of experimental results.

Material	Angle of Incidence (deg)	Orientation of Fringes[a]	Polarization	Spacing (μm)	Fluence of formation (J/cm^{-2})	Normalized formation fluence (J/cm^{-1})
Ge	75	Perpendicular	*P*	0.78	0.84	0.37
	75	Parallel	*P*	3.28	1.28	0.56
	75	Parallel	*P*	4.11[b]		
	60	Parallel	*P*	1.56	0.66	0.50
	45	Parallel	*P*	0.80	0.60	0.54
	30	Parallel	*P*	0.50	0.60	0.58
	70	Parallel	*S*	3.72	2.21	0.29
	70	Perpendicular	*S*	8.30[c]		
	60	Parallel	*S*	1.92	0.82	0.22
Al	75	Parallel	*P*	2.26	3.09	1.32
	60	Parallel	*P*	1.38	1.74	1.41
	45	Parallel	*S*	0.80	2.55	1.26
	45	Perpendicular	*S*	2.00[c]		
	30	Parallel	*S*	0.50	1.61	1.19

[a]Fringe orientation is measured relative to the direction of **kp** for each polarization.
[b]Fringes formed in the center of damage site on a liquid pool, see text.
[c]*b*-type fringes formed by "intensity interference." See Sec. VI.

LIPSS patterns, variably spaced wavelike structures propagating essentially radially outwards from the center of the damage site were observed. The spacing of these patterns, which was between 1 and 3 μm near the center and well below 1 μm towards the edge of the damage zone, showed no dependence on either the angle of incidence or the polarization of the incident light. However, the formation fluence and the definition of the ripples was dependent upon both the above parameters and the number of shots incident on the target. Typically these structures covered a large part of the site and were observed to form over a finite distance starting some way from the center. For reasons primarily based on the lack of angular dependence of the ripple spacing these patterns are attributed to ICW which are frozen into the surface upon resolidification.

C. ALIPSS

In the course of attempting to generate LIPSS we performed the same experiments at fluences two, three, or more times higher than the formation fluences in Table I. At these high fluences the interaction of the excimer with the target produced a large volume of plasma (many times that seen at lower fluences) accompanied by an audible cracking sound. The results under these conditions were badly damaged sites with a variety of complex structures of various orientations and spacings varying from less than 1 to more than 20 μm. In general these structures showed no simple dependence of their morphology, spacing, and orientation on either the fluence or the angle of incidence and polarization of the incident light.

However, for certain fluences and numbers of shots, structures whose orientation and dependence on angle of incidence was identical to that of p^- and c-type fringes, but with a much larger spacing, were observed. These anomalous structures are labeled as anomalous laser-induced periodic surface structures. Figure 8 shows such structures generated on an Al sample by P-polarized light incident at 60° of fluence 3.5 J cm^{-1}, where two sets of ripples, one with a grating vector parallel to **kp** labeled as p^{*-} type of spacing 10 μm and the other with a grating vector perpendicular to **kp** labeled as c^* type with a spacing of ≈ 3 μm, can be seen. The ratio of the ripple spacings is 3.3 whilst their morphology is similar to that observed for ripples formed on a liquid Ge surface.

IV. THEORY

A. LIPSS

The theory developed in I is based on a formal solution of Maxwell's equations and yields an expression for the inhomogeneous deposition of energy into a material which results from interference between the incident laser beam and fields scattered from microscopic surface roughness. The solution is based on an integral transform method developed by Sipe some years earlier and allows the inhomogeneous energy deposition into a material at a given value of induced wave vector as a function of angle and polarization to be found. The final expressions

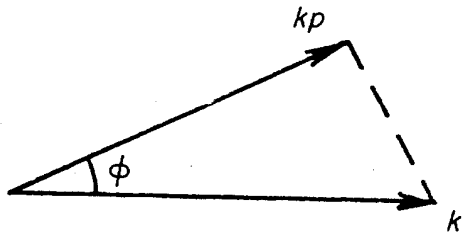

FIG. 3. Definition and orientation of angle ϕ.

have only two adjustable factors known as the shape (s) and filling factors (f). The f factor corresponds to the fraction of the available volume that the rough surface occupies, whilst the shape factor is derived from the way in which the rough surface was modeled, and essentially relates the width of any occupied area to the depth of roughness within that area. Following II, values of 0.1 for s and 0.4 for f were used in almost all calculations.

It is shown (I) that the inhomogeneous absorption of energy can be written as the product of two terms. Of these, one is a slowly varying function of **k**, where **k** is the induced surface wave vector (normalized to the incident wave vector) and can be ignored, whilst the other term known as the efficacy factor, depends upon both **k** and **kp**, and exhibits sharp peaks. It is argued that LIPSS formation is most likely at wave vectors corresponding to peaks in the efficiency factor. For clarity, it is worth noting that once ripples have formed, **k** and the so-called grating vector are one and the same. Following II we introduce the angle ϕ defined as the angle between **kp** and the induced wave vector **k** as in Fig. 3. Graphs of the efficacy factor, $\eta(\mathbf{k},\mathbf{kp})$, as a function of **k**, angle ϕ, and angle of incidence for various materials were plotted for both S- and P-polarized light (Figs. 4–6). In these calculations a complex refractive index[17] (n_c) of $4.0+i0.1$ (at

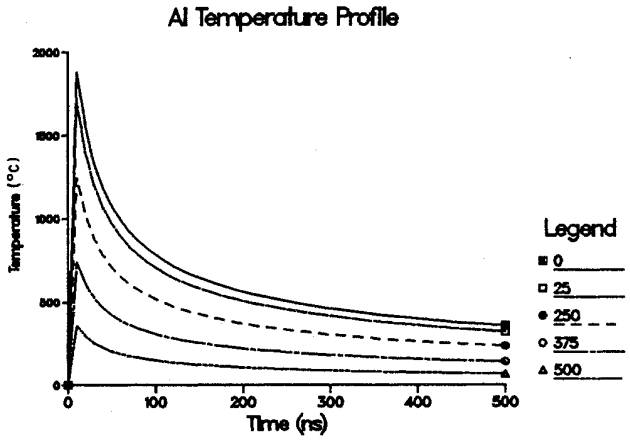

FIG. 4. The temperature profile on an Al block as a function of distance (in μm) from the center of the heat source (which is assumed to be a circularly symmetric Gaussian profile) and elapsed time (in ns) at a depth of 1 μm below the surface. The spot size of the Gaussian is 500 μm. The number under the legend refers to the distance in μm from the center of the irradiated area.

1060 nm) and $1.4+i3.2$ (at 249 nm) was used for Ge together with $0.2+i2.9$ (at 249 nm) for Al. The main omission in this theory is the neglect of any feedback mechanism either inter- or intrapulse whereby once preferential coupling at a given **k** value has begun, the process can be reinforced to yield LIPSS. This is discussed in detail in III.

Unfortunately, the above theory predicts only possible LIPSS spacings and gives no information on either the ripple morphology or the mechanism that actually causes a surface to deform leading to the ripple patterns. As a result of studies initially done by Emmony *et al.*[18,19] and more recently van Driel *et al.*[20] it appears that LIPSS formation is dependent on the total energy adsorbed rather than on the details of how the energy is actually absorbed and that the actual rippling of a surface occurs upon resolidification with a morphology that depends strongly upon the degree of surface melting. Whilst full details can be found elsewhere,[21] it is useful to state two conclusions from the previously mentioned works which are (1) on surfaces that are inhomogeneously melted, i.e., where melting occurs only in the immediate vicinity of areas of peak inhomogeneous energy absorption, narrow, sharply peaked, ripples will be formed and (2) on homogeneously, i.e., uniformly melted surfaces wide, almost sinusoidal, ripples are formed.

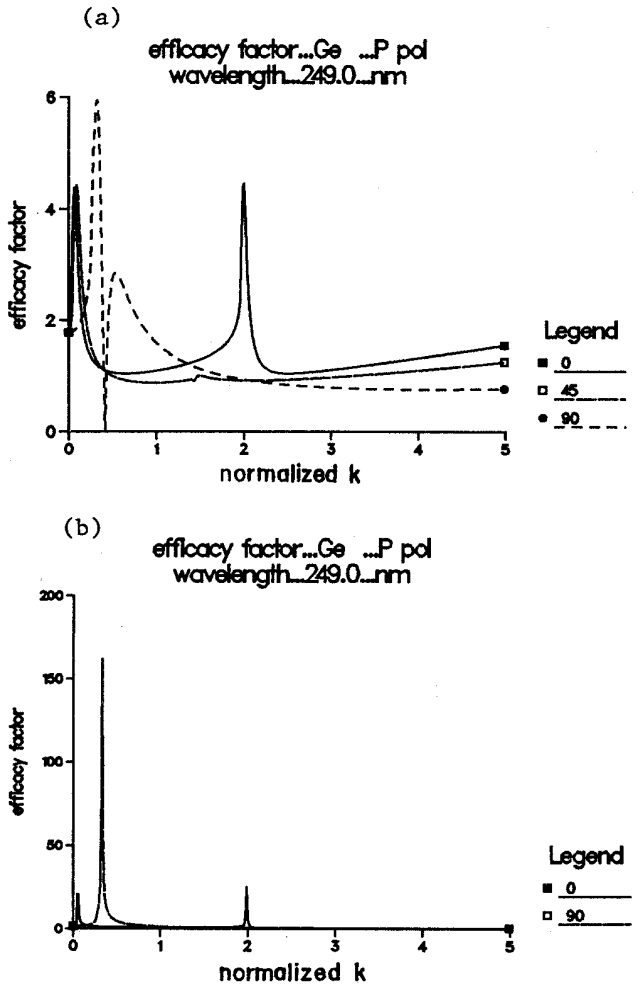

FIG. 5. Efficacy factors as a function of normalized k and angle ϕ for Ge under P-polarized 249-nm radiation at 75° incidence. The number under the legend is the ϕ angle in degrees. (a) Solid Ge with optical properties $n_c=1.4+i3.2$ and surface properties $s=0.4$, $f=0.1$. (b) Liquid Ge with optical properties $n_c=0+i5$.

B. ICW

Capillary waves which have well-known dispersion and decay time relationships[22] can be induced on a uniformly molten surface as a consequence of laser irradiation.[23] Previously reported structures[8,24] have been identified as surface plasmon excited capillary waves and are known as laser-induced capillary waves (LICW). The period of these structures is determined by the surface plasmon produced at the liquid and/or air interface which in turn depends upon the angle of incidence and polarization of the incident laser beam.

Given the above dependence of the spacing of LICW, this mechanism cannot explain the structures of Sec. III B where the spacing is independent of both the angle of incidence and polarization of the incident excimer pulse. It is our contention that the waves of Sec. III B are capillary waves generated as a result of the impulse that the surface suffers when material is ablated from it. This impulse would seed capillary waves in much the same way that dropping a stone into a lake generates waves. Under these conditions the ripple spacing is determined primarily by how long the impulse lasts, which in turn depends largely on how long the surface is molten rather than on either the angle of incidence or polarization of the incident laser beam.

In order to permanently record ICW the surface must freeze before the wave motion has decayed away and it has been suggested that this means that the time the surface is molten must be short compared to the decay time. Whilst this criteria would certainly freeze some pattern on the surface, it is our contention that to record an essentially undistorted profile, the freezing time must be short compared to the period of oscillation of the wave.

In order to allow at least qualitative discussion of the experimentally observed structures, an approximate profile of the temperature distribution in the sample is required. The model used is that proposed by Ready.[25] This analysis, which assumes temperature independence of the thermal properties, was carried out for Al only, as Ge being a semiconductor has a very strong variation of thermal properties with temperature. Details of the analysis and values of the relevant material parameters can be found in Ref. 21. Although this model makes no allowance for phase changes, this is not too serious since we are only interested in a very approximate estimate of how long the surface remains molten. Inclusion of phase changes, e.g., melting, would increase the time it takes the surface to initially become molten due to having to supply enough energy to overcome the latent heat of

melting. However, on cooling, the surface would remain molten longer as the energy associated with the latent heat of melting has to be removed. To first order these two times would be similar and thus tend to cancel with the result that an estimate of the time that the surface is molten can be made from a model which neglects phase changes. Since it is our intention merely to show the general trends in the temperature profile, and as estimates of the depth of the capillary waves suggested depths of around 1 μm, the data presented (Fig. 4) is based upon the temperature 1 μm below the surface.

C. Formation fluences

Under the assumption that LIPSS formation depends only on the total absorbed energy we have calculated a normalized energy of formation which makes allowance for the variation with angle of incidence of both the absorbed energy and the beam-target interaction area. The variation in energy absorption was allowed for by using the Fresnel-reflectivity coefficients, whilst that in the beam-target interaction area was allowed for by reference to the angle of incidence of the excimer beam. Using the

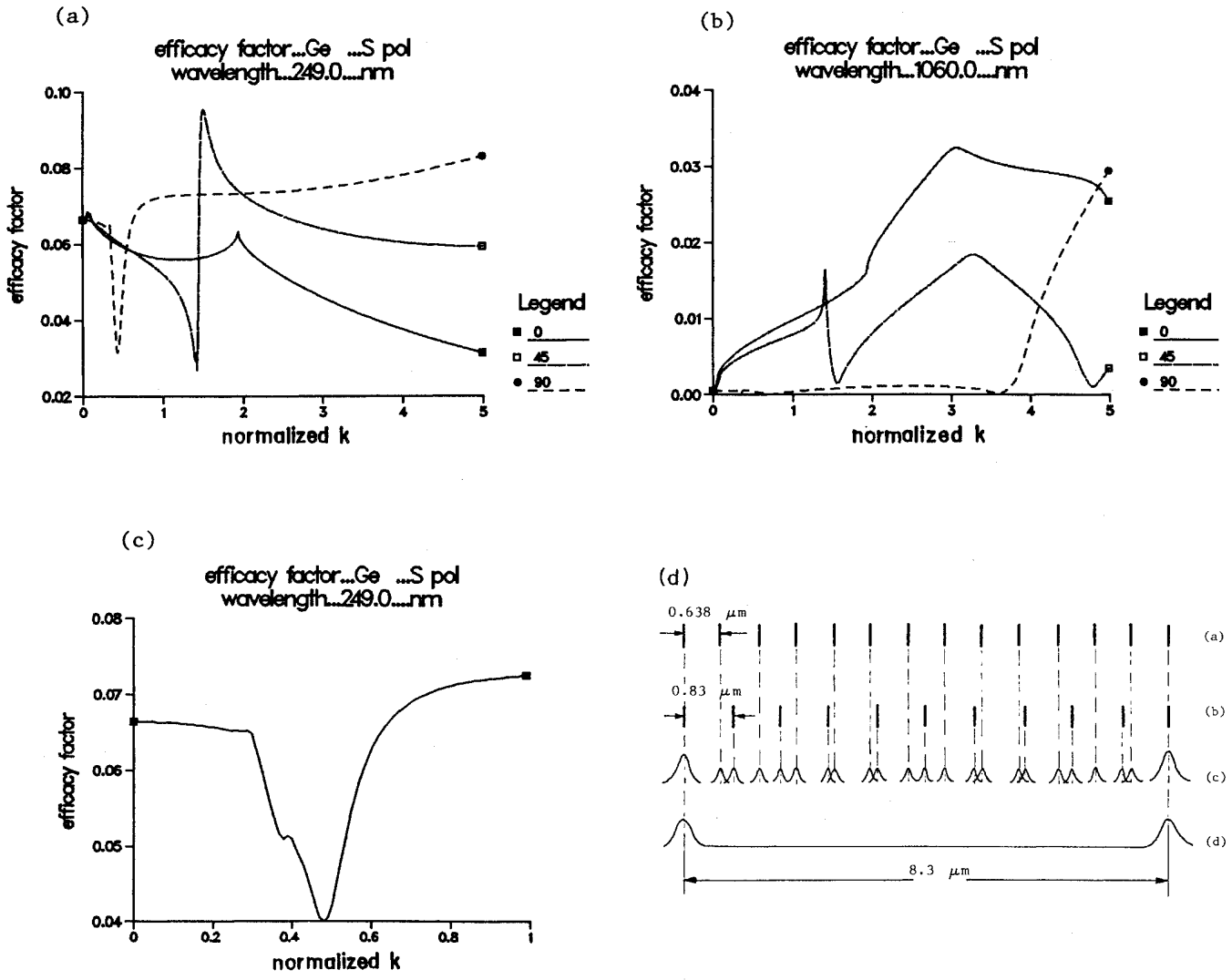

FIG. 6. Efficacy factors as a function of normalized k and angle ϕ for Ge under S-polarized radiation at 70° incidence with surface properties $s=0.4$, $f=0.1$. The number under the legend is the ϕ angle in degrees. (a) At 249 nm with $n_c=1.4+i3.2$, (b) at 1060 nm with $n_c=1.4+i3.2$, (c) at 249 nm with $n_c=1.4+i3.2$ and $\phi=87°$. Note how the change to metallic behavior [Figs. (a) and (b)] results in well-defined peaks appearing in η. Also note the closely spaced double peak in Fig. (c). In (d), (*a*) melt locations for the 0.39k wave, (*b*) melt locations for the 0.30k wave, (*c*) height of curve indicates the amount of surface melting. Note double melting at the start and when the melt locations of the waves overlap, (*d*) after multiple shot irradiation, ripples form at points of double melting.

experimentally obtained formation fluences and appropriate values of n_c, the results of these calculations are shown in Table I under the heading of normalized formation fluence.

V. COMPARISON OF THEORY AND EXPERIMENT

A. LIPSS s^-, p^-, and c ripples

Figures 5–7 are the efficacy factors for selected angles of incidence and polarization of the incident light. The traces for $\phi=0°$ correspond to **k** (i.e., a grating vector) being parallel to **kp**, i.e., s^- and p^- fringes, whilst $\phi=90°$ is for **k** perpendicular to **kp**, i.e., c-type fringes. By taking the value of **k** that produces the peaks in such graphs Table II was constructed and shows the experimental and theoretical fringe spacings and orientations in terms of **k** for all experimentally observed s^-, p^-, and c-type fringes. Table II shows that the theory for the inhomogeneous energy deposition is in very good agreement with what is found experimentally, which considering all the approximations used in obtaining the expressions, particularly the neglect of feedback processes and temperature dependence of any of the optical constants, is very satisfying.

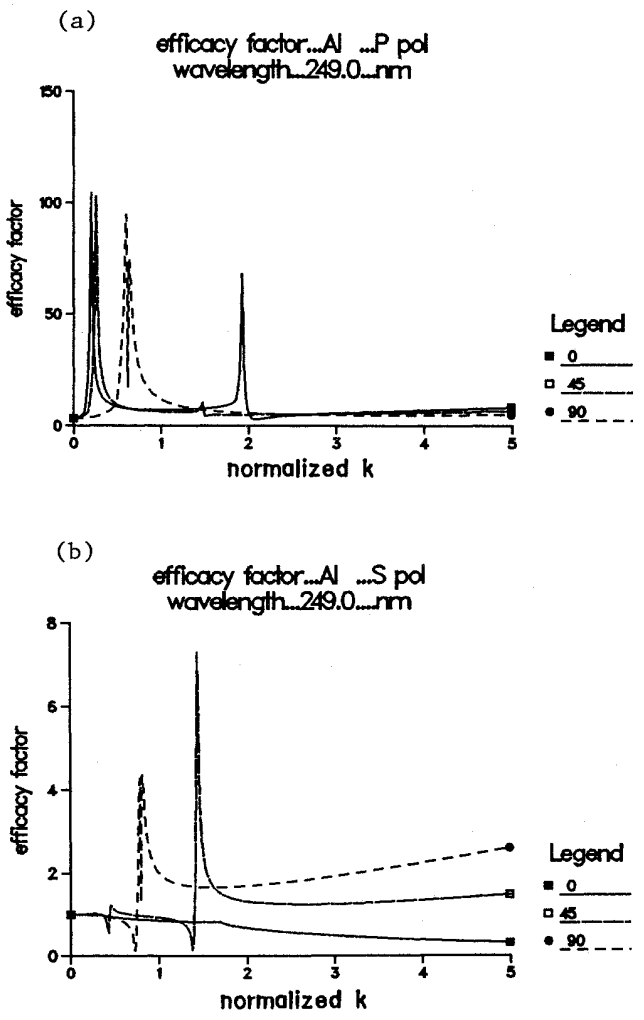

FIG. 7. Efficacy factor as a function of normalized k and angle ϕ for Al under 249-nm radiation with optical properties $n_c=0.2+i2.9$ and surface properties $s=0.4$, $f=0.1$. The number under the legend is the ϕ angle in degrees. (a) P polarized, 60° incidence, (b) S polarized, 45° incidence.

Despite many replicas being made, the subwavelength structures (e.g., p^+ and s^+) occur much less frequently than their larger-spaced counterparts. This could be due to a number of causes: (1) The extreme difficulty of observing the fringes because of their very shallow profile with the consequence that the samples have to be tilted at quite large angles to make the fringes observable, thereby reducing the likelihood of seeing the fringes even if they are present (2) A different threshold fluence for formation of the smaller fringes than for the larger fringes: (3) A tendency during the formation of the larger-spaced ripples to destroy (wash out) the smaller structures. (4) The influence of feedback on the size of the formed fringes. It is conceivable that once feedback is allowed for, the larger-spaced structures would be found to be more likely to occur.

The theory predicts not only fringes with a grating vector parallel to **kp** for both S and P polarizations, but more interestingly, and confirmed by experiment, the existence of the uniform c-type fringes for P-polarized light only. Unfortunately the theory cannot satisfactorily account for why the c-type fringes are so uniform or so dominant at the correct energy and it totally fails to explain their absence on Al. These problems are probably linked to the feedback mechanisms operative in each case. It is interesting to compare the uv (249 nm) and IR (1060 nm) efficacy factors for s-polarized light [Figs. 6(a) and 6(b)] where it can be seen that the transition from behaving optically as a dielectric at 1.06 μm to a metal at 249 nm allows new surface modes to exist that have definite peaks and result in the readily observed S-polarized LIPSS. Figures 6(a) and 7(b) show that the peaks representing the $s^\pm$ fringes are very slight, and again the reason that the $s^\pm$ fringes appear so strongly in practice is probably linked to feedback mechanisms, which also may explain the lack of $s^\pm$ fringes at certain angles.

In general, the fringes formed with a morphology similar to the narrow sharply peaked structures shown on the left-hand side of Fig. 1. Such ripples are consistent with the surface having inhomogeneously melted and have a spacing determined by the solid-state optical constants. However, it was possible to form regular structures with a more sinusoidal morphology such as those shown on the right-hand side of Fig. 1. Figure 2 shows that the ripple spacing varies in the vertical direction, being largest at the bottom of the picture which is nearest to the center of the excimer beam than at the top where the spacing is somewhat less. The effect is attributed to the variation in the optical constants of Ge with temperature. Since the morphology of the ripples remains the same as the spacing varies, it is our contention that all these ripples were

formed by localized (inhomogeneous) melting (and subsequent resolidification) but with the surface fields being initiated at different temperatures. Since Ge is a semiconductor, its optical constants will have a very strong temperature dependence, becoming more metallic as the temperature increases due to the increasing number of conduction-band electrons. This variation in the optical constants manifests itself as a variation in the wavelength of the surface fields which, when they interfere, result in a slight variation in the separation of the peaks and hence in ripple spacing. Calculations of the efficacy factor of Ge as its dielectric constant becomes more negative, i.e., metallic, show that the predicted ripple spacing increases slightly in agreement with the aforementioned proposal.

The broad near sinusoidal fringes such as those observed on the right-hand side of Fig. 1 were formed on a uniformly melted surface as a result of the freezing in of surface-plasmon-generated capillary waves (LICW). The spacing of the structures will be determined by the surface plasmon generated on a molten Ge surface. Calculations of the peak in the efficacy factor (i.e., the induced surface plasmon) using estimates[21] of the complex refractive index of liquid Ge in the uv based on a free-electron model yield ripple spacings in good agreement with experiment (Table II).

B. LIPSS *b* ripples

The origin of the well-defined large-spacing *b*-type fringes that occur with *S*-polarized light was initially unclear. Calculations of η for ϕ angles of 85°–90° using different values of the shape (s), filling factors (f), and optical constants failed to reveal peaks at the extremely small **k** values that these widely spaced ripples correspond to. However, for $\phi \neq 90°$ the efficacy factor has two closely spaced peaks. Figure 6(c) shows η for *S*-polarized light incident on Ge at 70° for $\phi = 87°$, with peaks at 0.3 and 0.39**k**. We suggest that the "waves" corresponding to these peaks "interfere" or beat with each other to give the observed ripples.

Figure 6(d) shows the positions on a surface at which the peaks in η would individually predict surface melting. The peaks at 0.3 and 0.39**k** correspond, respectively, to spacings of 0.83 and 0.638 μm as shown in the diagram. If the "waves" start at the same point, the location of the melting is usually different for each wave, but it is possible that after a sufficient number of periods (which will be different for each wave) the melt locations will once more overlap. In the case shown this occurs after 10 periods of the 0.3**k** wave, i.e., 8.3 μm, which corresponds exactly to 13 periods of the 0.39**k** wave. Hence, every 8.3 μm the amount of melting (to first order) will be doubled. On a shot-to-shot basis it does not seem unreasonable to argue that due to this increased melting, more of the incident energy is coupled into these areas than into the areas where the melting is due to only one wave. Thus after multiple shot irradiation the most likely structures to have formed are those with a spacing corresponding to the distance between the points of double melting. Reference to Fig. 5(c) shows that the spacing of these *b*-type fringes if 8 μm, in very good agreement with the above mechanism.

As a result of the problems in obtaining TEM and SEM images of rippled surfaces it proved impossible to determine whether or not structures corresponding to the individual waves that we suggest combine to yield the *b*-type ripples were present. Calculations for Al revealed a double peak in η that for $\phi = 86°$ occurred at 0.75 and 0.87**k**. If allowance for the approximate nature of the calculation is made and the above ideas are applied,

TABLE II. Comparison of theory and experiment.

Angle	Experimental Orientation[a]	Experimental **k**[b] measured	Theoretical Angle ϕ	Theoretical **k**[c] calculated
Ge *P* polarization				
75	Perpendicular	0.32	90	0.32
	Parallel	0.08	0	0.07
	Parallel[d]	0.06	0	0.06
60	Parallel	0.16	0	0.17
45	Parallel	0.31	0	0.32
30	Parallel	0.50	0	0.54
Ge *S* polarization				
70	Parallel	0.07	0	0.06
60	Parallel	0.13	0	0.14
Al *P* polarization				
75	Parallel	0.11	0.	0.10
60	Parallel	0.18	0	0.20
Al *S* polarization				
45	Parallel	0.31	0	0.31
30	Parallel	0.51	0	0.50

[a]Orientation measured relative to **kp**.
[b]All **k** values normalized to incident wave vector.
[c]Quoted value corresponds to the peak of the $\eta(\mathbf{k})$ vs **k** graph for the stated ϕ.
[d]Fringes on liquid surface with liquid dielectric constants.

values of 0.75 and 0.87**k** are almost exactly consistent with a spacing of 2 μm. Reference to Table I shows the spacing of the experimentally obtained ripples to be 2 μm, giving further support to the proposed mechanism. A detailed account of these new *b*-type ripples can be found in Ref. 26.

C. ICW

Figure 4 shows that at the energies used, the maximum time that the Al surface (melting point 660 °C) is molten is 200 ns but that further out towards the $1/e^2$ points the surface may only be molten for some tens of ns or less. Table III shows the calculated values of the spacings and decay times of the capillary waves as a function of the interaction time (ti). The interaction time ti is the time the surface remains molten and is determined from graphs such as Fig. 4. The frequency of the induced capillary wave (f_{cap}) is related to the interaction time by the first-order approximation $f_{\text{cap}} = 1/(2\ \text{ti})$. It can be seen from Table III that the short-wavelength structures have the fastest decay and that interaction times comparable to the time that the surface is molten (up to 200 ns) produces spacings consistent with those observed experimentally.

In the center of a damage site where the surface is molten longest, the short-wavelength structures will have decayed before resolidification leaving only larger-space ripples. Towards the edges of a damage site, where the surface is molten for a shorter time, short-wavelength structures will be observed as they will not have decayed before the surface solidifies. Attributing these structures to ICW cannot be fully justified without measurements of frequency and decay times which we could not do, but this attributation is at least consistent with that observed experimentally.

D. ALIPSS

Calculation of the peaks in the efficacy factor for Al with *P*-polarized light incident at 60° predict spacings of 1.25 μm parallel to **kp** and 0.39 μm perpendicular to **kp**, i.e., a ratio of 3.25 in the spacing of the two types. Although the spacing of both sets of experimental ripples (Fig. 8) is too large (by approximately the same factor of times eight), the ratio of their spacings (3.3) is in good agreement with that predicted above.

TABLE III. Wavelength-decay times for capillary waves. Note that ti is the interaction time of the liquid surface with the driving force.

ti ns	Wavelength (μm)	Decay time ns
1	0.2	1.2
5	0.6	11.0
10	1.0	28.0
20	1.5	70.0
30	2.0	120.0
100	4.5	600.0
200	7.1	1500.0

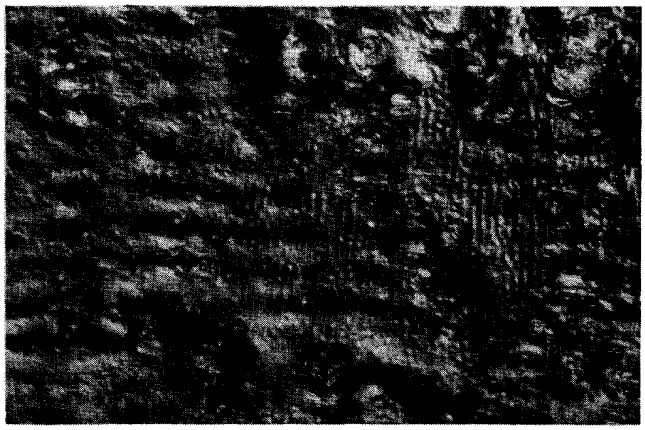

FIG. 8. ALIPSS on Al sample *P*-polarized light incident 60°, magnification XM 1250. Observe the p^{*-} (horizontal with large spacing) and c^* (vertical and of smaller spacing) ripples. Ripple morphology is similar to normal LIPSS but the spacing is about eight times too big.

As calculations using large and negative dielectric constants reveal that the efficacy factor is remarkably independent of the shape and filling factors, i.e., the surface parameters, we feel that to first order it is not unreasonable to ignore the undoubted effect that the presence of a plasma above a surface has on the surface itself. Instead, to first order, we treat the plasma simply as a medium that modifies the refractive index of the region immediately above and in contact with the test surface. Assuming that, at the fluences used, the plasma temperature, electron density, etc., are sufficiently low that the plasma can be treated as a free-electron gas, it is possible at certain frequencies to have a refractive index n (where $n = \epsilon^{1/2}$) of less than 1. Consider the situation where light of wavelength λ_a and thus frequency f_a (in air) is incident on a region of plasma immediately above the surface. To satisfy the boundary conditions the frequency must be the same in both media and hence the wavelength in the plasma λ_p is given by $\lambda_p = \lambda_a / n_p$, where n_p is the refractive index of the plasma. Hence if $n_p < 1$ the wavelength in the plasma, and thus that seen by the sample surface, is longer than that of the original laser irradiation.

In order to quantify the above idea an estimate of the electron density of the plasma that was associated with the formation of these ripples is required. The number of generated electrons obviously depends upon the number of incident photons and the efficiency with which an incident photon generates a free electron. Whilst accurately determining the number of free electrons requires detailed knowledge of the surface electrodynamics, we feel that for the purposes of an estimate it does not seem unreasonable to assume that the number of free electrons is 50% of the number of incident photons. In the case of the ripples shown in Fig. 8, the ripples covered an area about 0.4 by 0.1 mm^2. Assuming the plasma produced by the laser pulse to be confined to the same area and taking its thickness to be 10 μm, then at the fluence used, a

free-electron approximation yields a refractive index of 0.16. This would result in the wavelength, seen by the surface, being approximately equal to six times the vacuum value. The purpose of this calculation is to show that at the fluences used, and with "reasonable" estimates of the plasma volume and the fraction of photons that generate electrons, the plasma frequency ωp and angular frequency ω of the incident light are nearly the same. The refractive index of the plasma is therefore much less than 1 and hence the wavelength of the light incident on the surface is mush larger than the free-space wavelength. It is thus our contention that these observed ripples (p^{*-} and c^* type) are LIPSS generated by a laser pulse whose wavelength as seen by the surface has been greatly increased due to passage through the plasma immediately above the surface and are thus labeled as ALIPSS.

E. Formation fluences

The agreement of the normalized formation fluences (Table I) is much better for Al than Ge, which we suggest can be explained, at least in part, by the temperature dependence of the optical constants of the materials. Germanium being a semiconductor will have a much stronger variation of n_c with temperature than Al, and if, as is quite probable, a significant fraction of the absorption occurs with the material in a heated state then the change in the optical constants will have a large influence on the threshold energies. Two clear trends can be seen in Table I. Firstly, there is a substantial difference between Al and Ge which, at least in part, will be due to their different normal incidence reflectivity and thermal properties. Secondly, and more difficult to explain, is the fact that for each material there is agreement of the values within either S or P polarization but not between them, with the formation fluence for S being lower than that for P, particularly for Ge. It is not unreasonable to suggest that this difference is due in some way to a difference in the coupling of the light into the material, but beyond this tentative statement we have no explanation of this effect. The good agreement within each polarization of the normalized formation fluence, in our view, confirms the basic idea that it is the absorbed fluence that is the important parameter in LIPSS formation and also gives support to the generally accepted idea that the ripples are formed on resolidification.

VI. CONCLUSIONS

We have shown that LIPSS can occur in the uv for semiconductors or metals. The results obtained have been shown to be in good agreement with the theory developed in I and, in particular, have demonstrated the existence of and explanations for two entirely new sets of fringes for S-polarized light whilst in the process subjecting the theory to a thorough testing. There are obvious inadequacies in the theory which are almost certainly linked to the lack of any feedback mechanism in the expressions. We have also drawn attention to the different regimes of LIPSS formation in terms of localized or uniform melting and suggested possible explanations. Evidence to explain the radial-like wave forms seen at various distances from the center of the damage site in terms of ICW is presented and is shown to be in broad agreement with experiment.

We plan to investigate the formation of LIPSS using pulsed laser diffraction and high-resolution Schlieren imaging techniques. For the longer term we plan to investigate the formation of LIPSS on low-index dielectric materials such as quartz and calcium fluoride as well as some of the "new" optical materials such as solgel.

ACKNOWLEDGMENTS

The authors which to acknowledge the assistance provided by Anita Hood, Frank Page, and John Bates in performing the optical microscopy, SEM, and TEM work, respectively.

[1]M. Birnbaum, J. Appl. Phys. **36**, 3688 (1965).
[2]D. J. Ehrlich and S. R. J. Brueck, Appl. Phys. Lett. **47**, 216 (1985), and references therein.
[3]R. M. Osgood, Jr. and D. J. Ehrlich, Opt. Lett. **7**, 385 (1982).
[4]J. E. Sipe, J. F. Young, J. S. Preston, and H. M. van Driel, Phys. Rev. B **27**, 1141 (1983).
[5]D. C. Emmony, R. P. Howson, and L. J. Willis, Appl. Phys. Lett. **23**, 598 (1973).
[6]Z. Guosheng, P. M. Fauchet, and A. E. Siegman, Phys. Rev. B **26**, 5366 (1982).
[7]J. F. Young, J. S. Preston, H. M. van Driel, and J. E. Sipe, Phys. Rev. B **27**, 1155 (1983).
[8]J. F. Young, J. E. Sipe, and H. M. van Driel, Phys. Rev. B **30**, 2001 (1984).
[9]P. A. Temple and M. J. Soileau, Nat. Bur. Stand. (U.S.) Spec. Pub. No. 462 (U.S. GPO Washington, D.C., 1976), p. 371.
[10]P. A. Temple and M. J. Soileau, IEEE J. Quantum Electron. **QE-17**, 2067 (1981).
[11]K. Keilmann and Y. H. Bai, Appl. Phys. A **29**, 9 (1982).
[12]M. Prokhorov, V. A. Sychugov, A. V. Tishchenko, and A. A. Khakimov, Pis'ma Zh. Tekh. Fiz. **8**, 961 (1982) [Sov. Tech. Phys. Lett. **8**, 415 (1982)].
[13]V. I. Emel'yanov, E. M. Zemskov, and V. N. Seminogov, Kvantovaya Electronka (Moscow) **11**, 2283 (1984) [Sov. J. Quantum Electron. **14**, 1515 (1984)].
[14]I. Ursu *et al.*, J. Appl. Phys. **58**, 3909 (1985).
[15]S. E. Clark *et al.*, Nat. Bur. Stand. (U.S.) Spec. Pub. No. 746 (U.S. GPO, Washington, D.C., 1985), p. 35.
[16]M. Rückert, Structure **8**, 3 (1984).
[17]Most values for optical constants taken from *Handbook of Optical Constants of Solid*, edited by E. D. Palik (Academic, New York, 1985).
[18]D. C. Emmony, N. J. Phillips, J. H. Toyer, and L. J. Willis, J. Phys. D **8**, 1472 (1975).
[19]L. J. Willis and D. C. Emmony, Opt. Laser Technol. p. 222 (1975).
[20]H. M. van Driel, J. E. Sipe, and J. F. Young, J. Lumin. **30**, 446 (1985).
[21]S. E. Clark, Ph.D. thesis, Loughborough University, 1988.
[22]L. D. Landau and E. M. Lifshitz, *Fluid Mechanics* (Pergamon,

New York, 1980).
[23]F. Keilmann, Phys. Rev. Lett. **51**, 2097 (1983).
[24]J. F. Young, J. E. Sipe, and H. M. van Driel, Opt. Lett. **8**, 431 (1983).
[25]J. F. Ready, *Effects of High Power Laser Radiation* (Academic, New York, 1971).
[26]S. E. Clark, N. C. Kerr, and D. C. Emmony, J. Phys. D **22**, 527 (1989).

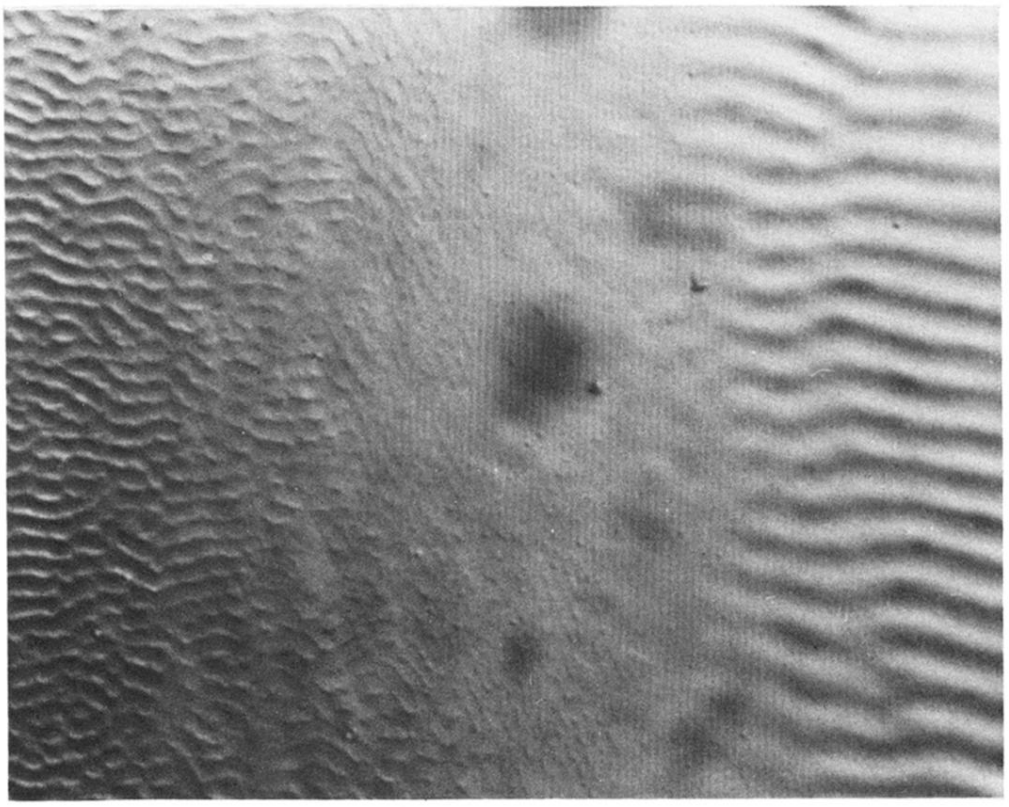

FIG. 1. Germanium sample, *P*-polarized light incident at 75°, magnification XM 2000. This micrograph shows both types of *p* fringes together with the extremely uniform *c* type orientated perpendicularly to the others. The ripples formed on the uniformly melted surface (right-hand side) appear to have a much flatter more sinusoidal shaped profile.

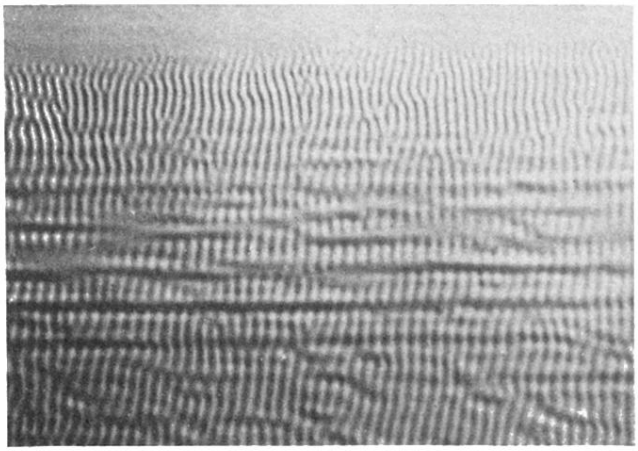

FIG. 2. Germanium sample, *S*-polarized light incident at 70°, magnification XM 1250. The variation of spacing vertically along the picture is believed to be associated with a varying dielectric constant due to a temperature gradient. Also note large near horizontal *b*-type fringes of spacing $\approx 8\,\mu$m.

FIG. 8. ALIPSS on Al sample *P*-polarized light incident 60°, magnification XM 1250. Observe the p^{*-} (horizontal with large spacing) and c^{*} (vertical and of smaller spacing) ripples. Ripple morphology is similar to normal LIPSS but the spacing is about eight times too big.